



# HHS Public Access

Author manuscript

*J Am Chem Soc.* Author manuscript; available in PMC 2017 April 27.

Published in final edited form as:

*J Am Chem Soc.* 2016 April 27; 138(16): 5341–5350. doi:10.1021/jacs.6b01706.

## A Synthetic Single-Site Fe Nitrogenase: High Turnover, Freeze-Quench $^{57}\text{Fe}$ Mössbauer Data, and a Hydride Resting State

Trevor J. Del Castillo<sup>†</sup>, Niklas B. Thompson<sup>†</sup>, and Jonas C. Peters<sup>\*</sup>

Division of Chemistry and Chemical Engineering, California Institute of Technology (Caltech), Pasadena, California 91125, United States

### Abstract

The mechanisms of the few known molecular nitrogen-fixing systems, including nitrogenase enzymes, are of much interest but are not fully understood. We recently reported that Fe-N<sub>2</sub> complexes of tetradentate P<sub>3</sub><sup>E</sup> ligands (E = B, C) generate catalytic yields of NH<sub>3</sub> under an atmosphere of N<sub>2</sub> with acid and reductant at low temperatures. Here we show that these Fe catalysts are unexpectedly robust and retain activity after multiple reloadings. Nearly an order of magnitude improvement in yield of NH<sub>3</sub> for each Fe catalyst has been realized (up to 64 equiv NH<sub>3</sub> produced per Fe for P<sub>3</sub><sup>B</sup> and up to 47 equiv for P<sub>3</sub><sup>C</sup>) by increasing acid/reductant loading with highly purified acid. Cyclic voltammetry shows the apparent onset of catalysis at the P<sub>3</sub><sup>B</sup>Fe-N<sub>2</sub>/P<sub>3</sub><sup>B</sup>Fe-N<sub>2</sub><sup>-</sup> couple and controlled-potential electrolysis of P<sub>3</sub><sup>B</sup>Fe<sup>+</sup> at -45 °C demonstrates that electrolytic N<sub>2</sub> reduction to NH<sub>3</sub> is feasible. Kinetic studies reveal first-order rate dependence on Fe catalyst concentration (P<sub>3</sub><sup>B</sup>), consistent with a single-site catalyst model. An isostructural system (P<sub>3</sub><sup>Si</sup>) is shown to be appreciably more selective for hydrogen evolution. In situ freeze-quench Mössbauer spectroscopy during turnover reveals an iron-borohydrido-hydride complex as a likely resting state of the P<sub>3</sub><sup>B</sup>Fe-catalyst system. We postulate that HER activity may prevent iron hydride formation from poisoning the P<sub>3</sub><sup>B</sup>Fe-system. This idea may be important to consider in the design of synthetic nitrogenases and may also have broader significance given that intermediate metal-hydrides and hydrogen evolution may play a key role in biological nitrogen fixation.

### Graphical Abstract

---

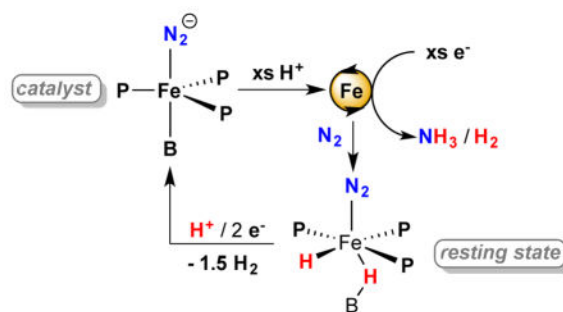
Corresponding Author: [jpeters@caltech.edu](mailto:jpeters@caltech.edu).

<sup>†</sup>**Author Contributions:** T.J.D.C. and N.B.T. contributed equally to this work.

The authors declare no competing financial interests.

Supporting Information

Experimental procedures and data for individual experiments. The Supporting Information is available free of charge on the ACS Publications website at <http://pubs.acs.org>.



## 1. INTRODUCTION

The fixation of molecular nitrogen ( $N_2$ ) into ammonia ( $NH_3$ ) is a transformation of fundamental importance to both biology and industry,<sup>1</sup> a fact which has prompted mechanistic study of the few known systems capable of catalyzing this reaction. The industrial Haber-Bosch process has been the subject of exhaustive investigation, resulting in a detailed mechanistic understanding in large part supported by surface spectroscopic studies on model systems.<sup>2</sup> The nitrogenase family of enzymes provides an example of catalytic  $N_2$  conversion under ambient conditions and has also been studied extensively. While many questions remain unanswered regarding the mechanism of nitrogenase, a great deal of kinetic and reactivity information has been collected.<sup>3</sup> Additionally, important insights have been provided by protein crystallography, X-ray emission spectroscopy, and site-mutagenesis studies, as well as in situ freeze-quench ENDOR and EPR spectroscopy.<sup>4,5</sup>

Hypotheses underpinning the mechanisms of both of these systems are bolstered by synthetic model chemistry and efforts to develop molecular  $N_2$  conversion catalysts.<sup>6</sup> This search has yielded systems capable of the catalytic reduction of  $N_2$  to hydrazine ( $N_2H_4$ ),<sup>7</sup> tris(trimethylsilyl)amine,<sup>8</sup> and a few examples of the direct catalytic fixation of  $N_2$  to  $NH_3$  (Chart 1).<sup>8,9,10,11,12</sup> While a wealth of mechanistic information for the original Mo catalyst system developed by Schrock has been derived from stoichiometric studies and theory,<sup>13,14</sup> in situ spectroscopic studies during catalysis were not reported. These synthetic catalysts operate under heterogeneous conditions and are likely to generate mixtures of intermediate species that are both diamagnetic and paramagnetic, making it challenging to reliably determine speciation under turnover. This latter limitation is also true of biological nitrogenases. While CW and pulsed-EPR techniques can and have been elegantly applied,<sup>5</sup> such studies are inherently limited in that species/intermediates not readily observable by these techniques will go unnoticed.

Iron is the only transition metal that is essential in the cofactor for nitrogenase function, and this fact has motivated a great deal of recent interest in Fe- $N_2$  model chemistry.<sup>15</sup> In recent years we have focused on a family of Sacconi-type tetradentate ligands,  $P_3^E$ , in which three phosphine donors are bonded to a central atom through an *ortho*-phenylene linker ( $E = B, Si, C$ ). We have shown that  $P_3^E M$  ( $M = Fe, Co$ ) complexes promote the binding and activation of  $N_2$ , as well as the functionalization of bound  $N_2$  with various electrophiles.<sup>16,17,18</sup> Moreover, we discovered that  $P_3^B Fe$  ( $P_3^B = \text{tris}(o\text{-diisopropylphosphinophenyl})\text{borane}$ ) and  $P_3^C Fe$  ( $P_3^C = \text{tris}(o\text{-diisopropylphosphinophenyl})\text{methyl}$ ) complexes mediate the catalytic

reduction of  $N_2$  to  $NH_3$  at low temperature using a strong acid— $[H(OEt)_2][BAr^F_4]$  ( $HBAr^F_4$ )—and a strong reductant—potassium graphite ( $KC_8$ ) (Chart 1, D).<sup>12</sup> One unique aspect of these Fe-based systems is their suitability for in situ spectroscopic study by freeze-quench  $^{57}Fe$  Mössbauer spectroscopy. In principle, this technique enables observation of the total Fe speciation as frozen snapshots during turnover.<sup>19</sup> For single-site Fe nitrogenase mimics of the type we have developed, analysis of such data is far simpler than in a biological nitrogenase where many iron centers are present.<sup>20</sup>

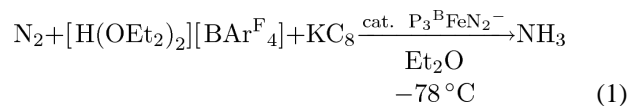
For the most active  $P_3^BFe$  catalyst system, many  $P_3^BFe-N_xH_y$  model complexes that may be mechanistically relevant (e.g.,  $Fe^+$ ,  $Fe-N_2^-$ ,  $Fe=NNH_2^+$ ,  $Fe-NH_3^+$ ) have now been independently generated and characterized, including by  $^{57}Fe$  Mössbauer spectroscopy, and these data facilitate interpretation of the freeze-quench Mössbauer data reported here. In combination with chemical quenching methods that we present to study the dynamics of product formation, it becomes possible to attempt to correlate the species observed spectroscopically with the  $N_2$  fixing activity to gain a better understanding of the overall catalytic system. Such a strategy complements the studies of model complexes and stoichiometric reactions steps that we have previously undertaken and offers a fuller mechanistic picture. While many questions remain, this approach to studying  $N_2$ -to- $NH_3$  conversion mediated by synthetic iron catalysts is a mechanistically powerful one.

Here we undertake tandem spectroscopy/activity studies using the  $P_3^E$  ( $E = B, C, Si$ ) Fe catalyst systems and report the following: (i) two of these Fe-based catalysts ( $E = B, C$ ) are unexpectedly robust under the reaction conditions, demonstrating comparatively high yields of  $NH_3$  that are nearly an order of magnitude larger than in initial reports at lower acid/reductant loadings; (ii) based on electrochemical measurements the dominant catalysis by the  $P_3^BFe$  system likely occurs at the formal  $P_3^BFe-N_2/P_3^BFe-N_2^-$  couple, corroborated by demonstrating catalysis with Na/Hg and electrolytic  $N_2$ -to- $NH_3$  conversion in a controlled-potential bulk electrolysis; (iii) the  $P_3^BFe$  system shows first order rate dependence on iron catalyst concentration and zero order dependence on acid concentration; (iv) kinetic competition between rates of  $N_2$  versus  $H^+$  reduction are a key factor in determining whether productive  $N_2$ -to- $NH_3$  conversion is observed; and (v) a metal hydride-borohydride species is a resting state of the  $P_3^BFe$  catalysis system.

## 2. RESULTS AND DISCUSSION

### 2.1. Increased turnover of Fe-catalyzed $N_2$ fixation and evidence for catalysis at the $P_3^BFe-N_2/P_3^BFe-N_2^-$ couple

Following our initial discovery that the addition of excess  $HBAr^F_4$  and  $KC_8$  to the anionic dinitrogen complex  $[P_3^BFe(N_2)][(12-crown-4)_2Na]$  (**1**) at low temperature in  $Et_2O$  under an atmosphere of  $N_2$  furnishes catalytic yields of  $NH_3$ , we pursued the optimization of this system for  $NH_3$  yield (Eqn. 1).



Under our initially reported conditions (in Et<sub>2</sub>O at -78 °C with 48 equiv HBAr<sup>F</sup><sub>4</sub> and 58 equiv KC<sub>8</sub>) the catalysis furnishes 7.0 ± 1.0 equiv of NH<sub>3</sub> per Fe atom, corresponding to 44% of added protons being delivered to N<sub>2</sub> to make NH<sub>3</sub>. Initial attempts at optimization showed that neither the overall concentration of the reactants nor the mole ratio of the catalyst substantially altered the yield of NH<sub>3</sub> with respect to proton equivalents.

We have since examined whether the post-reaction material retained any catalytic competence when more substrate was delivered. We found that if, after stirring at -78 °C for 1 hour the reaction mixture was frozen (at -196 °C), delivered additional substrate, and then thawed to -78 °C, significantly more NH<sub>3</sub> was formed. Iterating this reloading process several times resulted in a steady increase in the total yield of NH<sub>3</sub> per Fe atom (Figure 1), demonstrating that some active catalyst remains at -78 °C, even after numerous turnovers. This result implies that the yield of NH<sub>3</sub> is limited by competitive consumption of substrate in a hydrogen evolving reaction (HER).

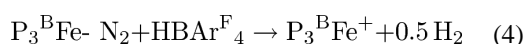
The apparent stability of at least some of the catalyst at low temperature suggested that it may be possible to observe higher turnover numbers if the catalyst is delivered more substrate at the beginning of the reaction. Indeed, as shown in Table 1, addition of increasing equivalents of HBAr<sup>F</sup><sub>4</sub> and KC<sub>8</sub> to **1** at low temperature furnished steadily increasing yields of NH<sub>3</sub> relative to catalyst, with a current maximal observed yield of 64 equivalents of NH<sub>3</sub> per Fe atom (average of 59 ± 6 over 9 iterations, Table 1, Entries 1–5) at 1500 equiv acid loading. This yield is nearly an order of magnitude larger than that reported at the original acid loading of 48 equiv. We note that the yields of NH<sub>3</sub> under these conditions are highly sensitive to the purity of the acid source, unsurprising given the high acid substrate loading relative to catalyst (~1500 equiv HBAr<sup>F</sup><sub>4</sub>). To obtain reproducible yields, we have developed a tailored protocol for the synthesis of sufficiently pure NaBAr<sup>F</sup><sub>4</sub>/HBAr<sup>F</sup><sub>4</sub>, which is detailed in the Supporting Information. It is also important to ensure good mixing and a high gas-liquid interfacial surface area to enable proper mass transfer in the heterogeneous reaction mixture.

Having discovered that P<sub>3</sub><sup>B</sup>Fe-N<sub>2</sub><sup>-</sup> **1** is a significantly more robust catalyst than originally appreciated, we investigated the activity of the alkyl N<sub>2</sub> anion [P<sub>3</sub><sup>C</sup>Fe-N<sub>2</sub>][(Et<sub>2</sub>O)<sub>0.5</sub>K] (**2**) toward N<sub>2</sub> fixation at higher substrate loading. Significantly higher yields of NH<sub>3</sub> per Fe are also attainable using **2** as a catalyst, albeit with roughly 2/3 the activity of **1** (Table 1, Entries 6–10). As a point of comparison, we also submitted the silyl congener [P<sub>3</sub><sup>Si</sup>Fe-N<sub>2</sub>][(12-crown-4)<sub>2</sub>Na] (**3**) (P<sub>3</sub><sup>Si</sup> = tris(*o*-diisopropylphosphinophenyl)silyl) to these conditions and observed dramatically lowered yields of NH<sub>3</sub>, consistent with earlier reports (Table 1, Entries 11,12). Although the P<sub>3</sub><sup>Si</sup>Fe-N<sub>2</sub><sup>-</sup> system **3** displays worse selectivity for NH<sub>3</sub> formation vs. HER than **1** (*vide infra*), **3** still demonstrates catalytic yields of NH<sub>3</sub> under sufficiently high substrate loading (up to 4 equiv NH<sub>3</sub> per Fe, Table 1 Entry 12).

Table 1 also contains data for catalytic trials with the borohydrido-hydrido complex  $(P_3^B)(\mu-H)Fe(H)(N_2)$  (**4-N<sub>2</sub>**) as a catalyst in mixed Et<sub>2</sub>O/toluene solvent. In the presence of admixed toluene **4-N<sub>2</sub>** is observed to be partially soluble and demonstrates competence as a catalyst (Table 1, Entry 14); in the absence of toluene **4-N<sub>2</sub>** shows poor solubility and lower than catalytic yields of NH<sub>3</sub> were observed under the originally reported catalytic conditions ( $0.50 \pm 0.1$  equiv NH<sub>3</sub> per Fe).<sup>12a</sup> The significance of these observations is discussed below (section 2.4).

The efficiency of NH<sub>3</sub> production with respect to acid substrate decreases under increasingly high turnover conditions for these iron systems. Our understanding of the HER kinetics (*vide infra*) rationalizes this phenomenon in that under comparatively low catalyst loading (which engenders higher turnover) the background HER should be increasingly competitive, thereby reducing N<sub>2</sub>-fixing efficiency. The product of the reaction (NH<sub>3</sub>) may also act as an inhibitor of catalysis. To test this latter possibility, catalytic runs with 150 equiv HBAr<sup>F</sup><sub>4</sub> and 185 equiv KC<sub>8</sub> in the presence of **1** were conducted with the inclusion of 25 equiv of NH<sub>3</sub> (Table 1, Entry 15). The fixed N<sub>2</sub> yield of this reaction is substantially lower than the comparable experiment without added NH<sub>3</sub> (Table 1, Entry 3). One contributing cause for NH<sub>3</sub> inhibition is that it sequesters HBAr<sup>F</sup><sub>4</sub> as [NH<sub>4</sub>][BAr<sup>F</sup><sub>4</sub>]; however, the yield of NH<sub>3</sub> observed in Entry 15 is suppressed compared to an experiment with only 100 equiv HBAr<sup>F</sup><sub>4</sub>. This observation indicates that NH<sub>3</sub> inhibits the catalytic reaction, and that the degree of inhibition is more substantial than stoichiometric leveling of the acid strength.

We also sought to establish the minimum reducing potential required to drive catalysis with P<sub>3</sub><sup>B</sup>Fe-N<sub>2</sub><sup>-</sup> **1**. We have shown in previous work that **1** reacts favorably with HBAr<sup>F</sup><sub>4</sub> in Et<sub>2</sub>O at -78 °C along a productive N<sub>2</sub> fixation pathway.<sup>18</sup> In brief, **1** can be doubly protonated in Et<sub>2</sub>O at -78 °C to generate P<sub>3</sub><sup>B</sup>Fe=NNH<sub>2</sub><sup>+</sup> (Eqn. 2). If only stoichiometric acid is present, **1** is instead unproductively oxidized to P<sub>3</sub><sup>B</sup>Fe-N<sub>2</sub> (Eqn. 3). We have only observed net oxidation in the reaction of the neutral P<sub>3</sub><sup>B</sup>Fe-N<sub>2</sub> state with HBAr<sup>F</sup><sub>4</sub> in Et<sub>2</sub>O to produce P<sub>3</sub><sup>B</sup>Fe<sup>+</sup> (Eqn. 4).



These observations suggest that N<sub>2</sub> fixing catalysis likely occurs at the P<sub>3</sub><sup>B</sup>Fe-N<sub>2</sub>/P<sub>3</sub><sup>B</sup>Fe-N<sub>2</sub><sup>-</sup> redox couple (-2.2 V vs Fc/Fc<sup>+</sup>), but not at the P<sub>3</sub><sup>B</sup>Fe<sup>+</sup>/P<sub>3</sub><sup>B</sup>Fe-N<sub>2</sub> couple (-1.5 V vs Fc/Fc<sup>+</sup>). We have explored this hypothesis via cyclic voltammetry (CV) experiments. Figure 2 shows electrochemical data for P<sub>3</sub><sup>B</sup>Fe<sup>+</sup> dissolved in Et<sub>2</sub>O at -45 °C under 1 atm N<sub>2</sub> in the presence

of 0.1 M NaBAR<sup>F</sup><sub>4</sub> as a soluble electrolyte to create a modestly conductive ethereal solution.<sup>21</sup> The blue trace shows the expected irreversible P<sub>3</sub><sup>B</sup>Fe<sup>+</sup>/P<sub>3</sub><sup>B</sup>Fe-N<sub>2</sub> couple centered around ~ -1.7 V and the P<sub>3</sub><sup>B</sup>Fe-N<sub>2</sub>/P<sub>3</sub><sup>B</sup>Fe-N<sub>2</sub><sup>-</sup> couple at -2.2 V, as previously reported.<sup>17a</sup> The red trace shows the electrochemical behavior of P<sub>3</sub><sup>B</sup>Fe<sup>+</sup> in the presence of 5 equiv HBAR<sup>F</sup><sub>4</sub>. The data reveal a sharp plateaued increase in current coincident with the P<sub>3</sub><sup>B</sup>Fe-N<sub>2</sub>/P<sub>3</sub><sup>B</sup>Fe-N<sub>2</sub><sup>-</sup> redox couple, and very little increase in current at the P<sub>3</sub><sup>B</sup>Fe<sup>+</sup>/P<sub>3</sub><sup>B</sup>Fe-N<sub>2</sub> couple. The onset of an apparent catalytic response at the P<sub>3</sub><sup>B</sup>Fe-N<sub>2</sub>/P<sub>3</sub><sup>B</sup>Fe-N<sub>2</sub><sup>-</sup> couple intimates that electrocatalysis may be feasible, and that chemical reductants with weaker reduction potentials than KC<sub>8</sub> may also be competent for N<sub>2</sub>-to-NH<sub>3</sub> conversion catalyzed by P<sub>3</sub><sup>B</sup>Fe-N<sub>2</sub><sup>-</sup>. Also, the potential of the apparent catalytic response does not shift from the P<sub>3</sub><sup>B</sup>Fe-N<sub>2</sub>/P<sub>3</sub><sup>B</sup>Fe-N<sub>2</sub><sup>-</sup> couple in the absence of acid, indicating that this reduction precedes the first protonation event.

To determine whether electrolytic N<sub>2</sub>-to-NH<sub>3</sub> conversion contributes to the catalytic feature observed in the CV data, a controlled-potential bulk electrolysis of P<sub>3</sub><sup>B</sup>Fe<sup>+</sup> and 10 equiv HBAR<sup>F</sup><sub>4</sub> in Et<sub>2</sub>O at -45 °C under 1 atm N<sub>2</sub> in the presence of 0.1 M NaBAR<sup>F</sup><sub>4</sub> electrolyte with a reticulated vitreous carbon working electrode was performed. The electrolysis was held at -2.6 V (vs Fc/Fc<sup>+</sup>) for 4.6 hours, after which time 5.85 C of charge had been passed. Product analysis revealed the formation of NH<sub>3</sub> (18% faradaic efficiency) as well as H<sub>2</sub> (58% faradaic efficiency). The amount of NH<sub>3</sub> generated in this experiment corresponds to 0.5 equiv with respect to Fe and 14% yield with respect to acid. When the experiment was performed at higher acid loading (50 equiv), the NH<sub>3</sub> yield increased substantially (1.4 equiv per Fe; 8% faradaic efficiency; electrolysis held at -2.3 V in this instance with 13.04 C charge passed over 9 hrs). While these yields of NH<sub>3</sub> with respect to Fe do not demonstrate formal turnover, they do suggest that electrocatalytic N<sub>2</sub>-to-NH<sub>3</sub> conversion by this iron system may be feasible. That the NH<sub>3</sub> yield increases with increased acid correlates well with our results in the chemical system. Studies to more thoroughly explore the electrocatalytic N<sub>2</sub>-to-NH<sub>3</sub> conversion behavior of P<sub>3</sub><sup>B</sup>Fe-species are underway.

The electrochemical data presented in Figure 2 also suggest that chemical reductants with weaker reduction potentials than KC<sub>8</sub> may be competent for N<sub>2</sub>-to-NH<sub>3</sub> conversion catalysis by **1**. Consistent with this notion we find that catalytic yields of NH<sub>3</sub> (5 equiv per Fe) are obtainable using **1** in the presence of 150 equiv HBAR<sup>F</sup><sub>4</sub> and 1900 equiv 10 wt% Na/Hg amalgam under ~1 atm N<sub>2</sub> at -78 °C in Et<sub>2</sub>O (Table 1, Entry 16; a larger excess of 10 wt% Na/Hg amalgam was employed to compensate for the lower surface area of the reagent). This result demonstrates that the catalysis is not unique to the presence of either potassium or graphite. KC<sub>8</sub> is a stronger reductant than is needed for N<sub>2</sub>-to-NH<sub>3</sub> conversion, but shows more favorable selectivity for N<sub>2</sub> reduction relative to H<sub>2</sub> generation than other reductants we have thus far canvassed.

## 2.2 Kinetics of ammonia and hydrogen formation

To better understand the competing NH<sub>3</sub>- and H<sub>2</sub>-forming reactions that occur during catalysis, we measured the time profiles of product formation using the most active catalyst, P<sub>3</sub><sup>B</sup>Fe-N<sub>2</sub><sup>-</sup> **1**. Our method for quenching catalytic NH<sub>3</sub> production uses rapid freeze-quenching of reactions to -196 °C, followed by addition of *tert*-butyllithium (*t*BuLi), and

subsequent annealing to  $-78$  °C. Employing this method allows for the measurement of  $\text{NH}_3$  production as a function of time. The time courses of  $\text{NH}_3$  formation obtained for the previously reported substrate loading (blue trace)<sup>12a</sup> as well as a higher substrate loading (red trace) are shown in Figure 3.

Under both substrate loadings shown in Figure 3, the reaction proceeds to completion at  $-78$  °C. Furthermore, under the higher-turnover conditions (with 150 equiv  $\text{HBAr}^{\text{F}_4}$  and 185 equiv  $\text{KC}_8$ , Figure 3, red triangles) the reaction proceeds to completion over  $\sim 45$  min, a time-scale that enables us to measure the dependence of  $d[\text{NH}_3]/dt$  on the concentrations of the soluble reagents—**1** and  $\text{HBAr}^{\text{F}_4}$ —via the method of initial rates. As shown in Figure 4 (left), an initial rates analysis demonstrates that the reaction is first order in  $[\text{Fe}]$ , which is consistent with the involvement of a monomeric  $\text{P}_3^{\text{B}}\text{Fe}$  species in the turnover-limiting step for  $\text{NH}_3$  formation. Comparing conditions ranging from 15 mM to 250 mM  $[\text{HBAr}^{\text{F}_4}]$  revealed no significant correlation between initial  $[\text{HBAr}^{\text{F}_4}]$  and initial  $\text{NH}_3$  production rate; for instance, there is no measurable difference in the amount of  $\text{NH}_3$  produced after five minutes. This observation suggests zero-order rate dependence on acid concentration, which is borne out by the initial rates analysis (Figure 4, right).

These data provide an estimate of initial turnover frequency (TOF, determined as moles of  $\text{NH}_3$  produced per minute per Fe atom) of this catalyst system of  $1.2 \pm 0.1 \text{ min}^{-1}$ . While the TOF of this catalyst is not directly comparable to other  $\text{N}_2$ -to- $\text{NH}_3$  conversion catalysts due to differences in conditions and substrate, it is notable that **1** under the conditions used here furnishes a substantially higher TOF than the other synthetic systems in Chart 1 for which data is available (Table 2), despite operating over 100 °C lower in temperature (albeit with the benefit of a stronger reductant). MoFe nitrogenase purified from *Klebsiella pneumoniae* exhibits a TOF of approximately  $80 \text{ min}^{-1}$ ,<sup>22</sup> nearly two orders of magnitude larger than the present synthetic Fe system, while operating at room temperature.

To determine potential HER activity of  $\text{P}_3^{\text{B}}\text{Fe-N}_2^-$  **1**, we measured the time course of  $\text{H}_{2(\text{g})}$  formation from  $\text{HBAr}^{\text{F}_4}$  and  $\text{KC}_8$  in the absence and presence of **1**, under catalytically relevant conditions. As shown in Figure 5, the initial rate of  $\text{H}_{2(\text{g})}$  evolution at  $-78$  °C is enhanced by the presence of **1**. The Fe-catalyzed HER is  $> 85\%$  complete within the first hour with a final yield of  $\sim 40\%$  (blue trace).<sup>23</sup> Quantifying the  $\text{NH}_3$  produced in this reaction (34% yield based on  $\text{HBAr}^{\text{F}_4}$ ) accounts for 74% of the acid added. We also confirm that there is significant background HER from  $\text{HBAr}^{\text{F}_4}$  and  $\text{KC}_8$  (black trace), as expected. We conclude that both catalyzed and background HER are competing with  $\text{NH}_3$  formation in the catalyst system.

As a point of comparison, we also measured the rate of  $\text{H}_2$  evolution in the presence of  $\text{P}_3^{\text{Si}}\text{Fe-N}_2^-$  (**3**). As shown in Figure 5, **3** also catalyzes HER, with an initial rate that is comparable to **1**. However, in this case,  $\text{H}_2$  evolution approaches completion over two hours, resulting in a final measured yield of 88%. This is consistent with the low  $\text{N}_2$ -fixing activity of **3**; in the absence of a competitive  $\text{NH}_3$ -producing reaction, **3** catalyzes the reduction of protons to  $\text{H}_2$ . Understanding the fundamental differences that give rise to the divergent selectivity of these Fe catalysts is an important goal in the context of designing selective  $\text{N}_2$  reduction catalysts.

### 2.3 Spectroscopic characterization of Fe speciation under turnover

Considering the relatively slow rate of  $\text{NH}_3$  formation ascertained from low-temperature quenching experiments, we sought to determine the Fe speciation under turnover using the  $\text{P}_3^{\text{B}}\text{Fe-N}_2^-$  catalyst **1**. By rapidly freeze-quenching reaction mixtures using  $^{57}\text{Fe}$ -enriched **1** as a catalyst, time-resolved Mössbauer spectra can be obtained reflective of catalysis.<sup>24</sup>

The Mössbauer parameters of some independently synthesized  $\text{P}_3^{\text{B}}\text{Fe}$  species that may be relevant to the present catalysis have been measured and are collected in Table 3. Mössbauer isomer shifts ( $\delta$ ) can often be used to assign the relative oxidation state of structurally related compounds,<sup>16b,25</sup> yet in this series of  $\text{P}_3^{\text{B}}\text{Fe}$  compounds there is a poor correlation between  $\delta$  and formal oxidation state assignments (e.g.  $\text{Fe-N}_2^-$  and  $\text{Fe=NNH}_2^+$  species have nearly identical isomer shifts). This fact reflects the high degree of covalency present in these  $\text{P}_3^{\text{B}}\text{Fe-N}_x\text{H}_y$  complexes, skewing classical interpretations of the Mössbauer data; the degree of true oxidation/reduction at the iron centers in  $\text{P}_3^{\text{B}}\text{Fe-N}_x\text{H}_y$  species is buffered by strong covalency with the surrounding ligand field.<sup>26,27</sup> We do, however, find a useful linear correlation ( $r^2 = 0.90$ ) between the measured ground spin states ( $S$ ) of  $\text{P}_3^{\text{B}}\text{Fe-N}_x\text{H}_y$  compounds and  $\delta$  (Figure 6),<sup>28</sup> providing an empirical relationship that guides analysis of Mössbauer spectra obtained from catalytic reactions. Ground spin states can be reliably correlated with the type of  $\text{N}_x\text{H}_y$  ligand, and possibly the presence of hydride ligands, coordinated to a  $\text{P}_3^{\text{B}}\text{Fe}$  center. This knowledge, combined with freeze-quench Mössbauer data, enables us to predict with some confidence the type(s) of Fe species that are present in a spectrum obtained after freeze-quenching during turnover.

Figure 7 shows time-resolved Mössbauer spectra of freeze-quenched catalytic reaction mixtures of  $\text{P}_3^{\text{B}}\text{Fe-N}_2^-$  anion **1** with 48 equiv of  $\text{HBAr}^{\text{F}}_4$  and 58 equiv of  $\text{KC}_8$ . Figure 7A shows the spectrum of catalyst **1** as a 0.64 mM solution in THF, which features a sharp, asymmetric quadrupole doublet at 80 K in the presence of a 50 mT external magnetic field. Figure 7B shows the spectrum of a catalytic reaction mixture freeze-quenched after 5 minutes of stirring, revealing the major Fe species (blue, representing ca. 60% of all Fe) present during active turnover to have parameters  $\delta = 0.16 \pm 0.2 \text{ mm s}^{-1}$  and  $E_{\text{Q}} = 1.63 \pm 0.03 \text{ mm s}^{-1}$ , which, within the error of the simulation, is consistent with the diamagnetic borohydrido-hydrido species  $(\text{P}_3^{\text{B}})(\mu\text{-H})\text{Fe}(\text{H})(\text{L})$  (**4-L**), where  $\text{L} = \text{N}_2$  or  $\text{H}_2$ .<sup>29</sup> This observation correlates well with the previously reported result that **4-N**<sub>2</sub> is produced from the reaction of **1** with smaller excesses of  $\text{HBAr}^{\text{F}}_4$  and  $\text{KC}_8$ .<sup>12a</sup> Further corroborating this assignment, data collected at liquid He temperature with a small applied magnetic field suggest that this species is a non-Kramer's spin system,<sup>30</sup> and should be  $S = 0$  given the observed correlation between  $\delta$  and  $S$  (*vide supra*). Also present in Figure 7B is a minor component (~8%, shown in white) with parameters  $\delta = 0.02 \pm 0.2 \text{ mm s}^{-1}$  and  $E_{\text{Q}} = 0.97 \pm 0.2 \text{ mm s}^{-1}$ , and a broad residual absorbance centered at  $\delta \approx 0.9 \text{ mm s}^{-1}$  encompassing a width of  $\sim 2 \text{ mm s}^{-1}$  (representing ca. 20–30% of all Fe in the sample, shown in grey). Due to the broadness of the latter resonance ( $\Gamma \approx 1 \text{ mm s}^{-1}$ ), this feature could not be accurately modeled. Nevertheless, the signal is consistent with several known  $S = 3/2$   $\text{P}_3^{\text{B}}\text{Fe}$  species. For example, the vacant cation,  $\text{P}_3^{\text{B}}\text{Fe}^+$ , and the cationic species  $\text{P}_3^{\text{B}}\text{Fe-N}_2\text{H}_4^+$  and  $\text{P}_3^{\text{B}}\text{Fe-NH}_3^+$ , are  $S = 3/2$  species and give rise to quadrupole doublets that lie within the envelope of this broad signal (Table 3, Entries 1–3).<sup>31</sup> The utility of freeze-quench  $^{57}\text{Fe}$  Mössbauer

spectroscopy is evident; in a single spectral snapshot the presence of  $P_3^BFe$ -components with varied spin states including  $S = 0, 1/2, 1,$  and  $3/2$  are observed.

Figure 7C shows that the primary Fe species present after 25 minutes of reaction time is the starting catalyst **1** (shown in red, representing ca. 70% of all Fe in the sample). Also present is ca. 20% of the species we assign as **4-L** ( $\delta = 0.22 \pm 0.2 \text{ mm s}^{-1}$  and  $E_Q = 1.62 \pm 0.03 \text{ mm s}^{-1}$ , shown in blue),  $< 5\%$  of the neutral dinitrogen complex,  $P_3^BFe-N_2$  (green), and  $\sim 7\%$  of an as-yet unknown species with parameters  $\delta = 0.00 \pm 0.02 \text{ mm s}^{-1}$  and  $E_Q = 2.97 \pm 0.06 \text{ mm s}^{-1}$  (white). Thus, as acid substrate is consumed in the reaction to produce  $NH_3$  and  $H_2$ , the mixture of Fe species shown in Figure 7B at an early time point evolves back to the starting material **1**. A slight residual excess of  $KC_8$  is needed to ensure recovery of the active catalyst. These data help rationalize the results of the substrate reloading experiments (*vide supra*).

The increasingly low Fe concentrations used to achieve the highest yields of  $NH_3$  reported here make the collection of well-resolved Mössbauer spectra under such conditions challenging. Nonetheless, we repeated freeze-quench experiments for one set of higher-turnover conditions (Figure 8). Although in this case the Fe speciation at intermediate times appears more complex, these data exhibit the same gross behavior shown in Figure 7; under active turnover the major Fe species present is consistent with hydride **4-L** ( $\sim 50\%$ , average parameters  $\delta = 0.20 \pm 0.2 \text{ mm s}^{-1}$  and  $E_Q = 1.49 \pm 0.09 \text{ mm s}^{-1}$ , Figure 8A,B<sup>32</sup>), and as the extent of reaction increases significant amounts of  $P_3^BFe-N_2^-$  **1** reform (Figure 8C<sup>33</sup>).

#### 2.4 Precatalyst activity of $(P_3^B)(\mu-H)Fe(H)(N_2)$ (**4-N<sub>2</sub>**) and identification of a catalyst resting state

The observations presented in section 2.3 suggest that hydride **4-L** builds up as the major Fe-containing species during active turnover and appears to be converted back to the active catalyst **1** when catalysis is complete. We previously observed that this species can form under conditions that model the catalytic conditions (10 equiv acid/12 equiv reductant) and our initial thinking that **4-N<sub>2</sub>** may be a catalyst deactivation product was guided by the poor activity of isolated **4-N<sub>2</sub>** as a precatalyst under the standard conditions (generating only  $0.5 \pm 0.1$  equiv  $NH_3$  per Fe at 50 equiv acid/60 equiv reductant).<sup>12a</sup> However, in that initial report we also noted that isolated **4-N<sub>2</sub>** is not solubilized under the catalytic conditions. Therefore, in light of the current in situ spectroscopy, and the observation that **4-N<sub>2</sub>** liberated some  $NH_3$  under the original conditions, we wondered whether its insolubility may be what is responsible for its comparative low activity as an isolated precursor. If **4-N<sub>2</sub>** is brought into solution, or formed in solution during turnover, it may exhibit activity. To test this hypothesis we explored the activity of **4-N<sub>2</sub>** under modified catalytic conditions where a toluene/ $Et_2O$  mixture (which improves the solubility of **4-N<sub>2</sub>**) was employed as the solvent. In this case we find that **4-N<sub>2</sub>** serves as a viable precatalyst (Table 1, Entries 13, 14). We suppose then that under the standard conditions (in pure  $Et_2O$ ), if **4-L** is generated in solution during catalysis, it should be able to react productively so long as it does not irreversibly precipitate, which may be slow at  $-78 \text{ }^\circ\text{C}$ . Accordingly, we have observed that the Mössbauer spectrum of a sample taken from a standard catalytic mixture as described in section 2.3 can be filtered at low temperature and still displays substantial **4-L**.

These results suggest the feasibility of the stoichiometric transformation of hydride **4-L** into  $N_2$  anion **1** under catalytically relevant conditions. In a previous report, we showed that **4-N<sub>2</sub>** is stable for short periods to either  $HBAr^F_4$  or  $KC_8$  in  $Et_2O$  at room temperature, again noting its insolubility under these conditions.<sup>12a</sup> Given the results above, we have reinvestigated this reactivity in  $Et_2O$ /toluene mixtures. Thus the reaction of **4-N<sub>2</sub>** with 1 equiv of  $HBAr^F_4$  in 6:1 *d*<sub>8</sub>-toluene: $Et_2O$  results in consumption of the starting material along with the appearance of several new, paramagnetically-shifted <sup>1</sup>H NMR resonances. We hypothesize that protonolysis of either the terminal or bridging hydride moieties in **4-N<sub>2</sub>** produces a cationic “ $P_3^BFe-H^+$ ” species, which may then be reduced to liberate 0.5 equiv of  $H_2$  and re-enter the catalytic manifold of  $\{P_3^BFe-N_2\}^n$  species under an  $N_2$  atmosphere. Indeed, the sequential addition of 1.5 equiv of  $HBAr^F_4$  followed by 6 equiv of  $KC_8$  to **4-N<sub>2</sub>** at  $-78$  °C in 3:1  $Et_2O$ :toluene produces substantial amounts of **1** (32% yield, unoptimized; Scheme 1). This stoichiometric reactivity provides support for the idea that as **4-L** is formed under the standard reaction conditions it can react with acid and reductant to produce the starting catalyst **1**, consistent with the observations provided in section 2.3.

Given that (i) **4-L** appears to be the predominant Fe-containing species observed by freeze-quench Mössbauer spectroscopy under turnover conditions at early time points, (ii) that this species serves as a competent precatalyst when solubilized, and (iii) **4-N<sub>2</sub>** can be synthetically converted to **1** by  $HBAr^F_4$  and  $KC_8$ , we conclude that **4-L** is a major resting state of the catalysis. This conclusion does not require **4-L** to be an “on path” intermediate; we instead think **4-L** is more likely a resting state that ties up the catalyst, but one that reversibly leaks into the on-path catalytic cycle in which **1** is ultimately protonated.

The observation of a hydride resting state for this synthetic Fe catalyst may have additional relevance in the context of biological nitrogen fixation, where the intermediacy of metal hydride species has been proposed on the basis of spectroscopic data obtained during turnover.<sup>5</sup> It has further been proposed that the reductive elimination of hydrides as  $H_2$  may be a requisite component of  $N_2$  binding to the nitrogenase active-site cofactor,<sup>22,34,35</sup> giving rise to obligate  $H_2$  evolution in the limiting stoichiometry of  $N_2$  conversion to  $NH_3$ .<sup>36</sup> The results described here directly implicate the relevance of a synthetic iron hydride species to a system capable of catalytic  $N_2$ -to- $NH_3$  conversion. This in turn motivates complimentary model reactivity studies on iron hydride species such as **4-L**, targets whose relevance might otherwise be overlooked.

## 2.5 Summary of mechanistically relevant observations

To help collect the information presented here and in related studies of the  $P_3^BFe$ -system, Scheme 3 provides a mechanistic outline for the key iron species and plausible transformations we think are most relevant to the catalytic  $N_2$ -to- $NH_3$  conversion cycle catalyzed by  $P_3^BFeN_2^-$  **1**. The complexes shown in blue, along with their respective spin states  $S$ , have been thoroughly characterized. Also, the net conversions between complexes that are indicated by solid blue arrows have been experimentally demonstrated. Those complexes depicted in black have not (as yet) been experimentally detected.

Several results are worth underscoring. (i) We have characterized the  $S = 3/2$ , substrate-free state  $P_3^BFe^+$ , and shown that it binds  $N_2$  upon electron loading, generating  $S = 1$   $P_3^BFe-N_2$  or  $S = 1/2$   $P_3^BFe-N_2^-$  depending on reducing equivalents provided.<sup>12a,17</sup>  $P_3^BFe^+$  is competent for catalytic  $N_2$ -to- $NH_3$  conversion,<sup>12a</sup> and facilitates this conversion electrolytically as established herein. (ii) The most reduced state,  $P_3^BFe-N_2^-$  **1**, can be doubly protonated at low temperature to generate  $P_3^BFe=N-NH_2^+$ , a distal pathway intermediate.<sup>18</sup> This  $S = 1/2$  species features a short Fe-N multiple bond ( $\sim 1.65$  Å). Its diamagnetic relative,  $P_3^{Si}Fe=N-NH_2^+$ , has very recently been structurally characterized.<sup>37</sup> (iii) The  $P_3^BFe=N-NH_2^+$  intermediate anneals (in the absence of reductant) to generate significant amounts of  $P_3^BFe-NH_3^+$ ;<sup>12a,18</sup> (iv)  $P_3^BFe-NH_3^+$  can also be generated by protonation of  $P_3^BFe-NH_2$ , and reductive displacement of  $NH_3$  from  $P_3^BFe-NH_3^+$  under  $N_2$  regenerates  $P_3^BFe-N_2^-$ .<sup>12a</sup>

Also worth emphasizing is that diamagnetic  $P_3^{Si}Fe=N-NH_2^+$  can be reduced at low temperature to  $S = 1/2$   $P_3^{Si}Fe=N-NH_2$ , and this species in the presence of additional acid and reductant evolves to a mixture of  $P_3^{Si}Fe-N_2H_4^+$  and  $P_3^{Si}Fe-NH_3^+$ .<sup>37</sup>  $P_3^{Si}Fe-N_2H_4^+$ , and also  $P_3^BFe-N_2H_4^+$ , readily disproportionate the bound  $N_2H_4$  to generate the corresponding  $NH_3$  adducts  $P_3^{Si}Fe-NH_3^+$  and  $P_3^BFe-NH_3^+$ ,<sup>12a,16b</sup> each of which evolves  $NH_3$  upon reduction to regenerate (under  $N_2$ )  $P_3^BFe-N_2^-$  **1** and  $P_3^{Si}Fe-N_2^-$ , respectively. The reaction pathway observed for  $P_3^{Si}Fe=N-NH_2^+$ , more readily studied than for  $P_3^BFe=N-NH_2^+$  because  $P_3^{Si}Fe=N-NH_2^+$  can be isolated in pure form, highlights the possibility of a hybrid crossover mechanistic pathway wherein a distal intermediate ( $Fe=N-NH_2$ ) traverses to an alternating intermediate ( $Fe-N_2H_4$ ) that may then be converted to  $NH_3$ , possibly via disproportionation.<sup>18,37</sup> By demonstrating first-order rate dependence on the concentration of  $P_3^BFe-N_2^-$ , [**1**], the present study remains consistent with our hypothesis that a single-site mechanism is likely operative during  $N_2$ -to- $NH_3$  conversion catalysis. The direct observation of both **1** and its neutral form  $P_3^BFe-N_2$  in catalytic mixtures by freeze-quench Mössbauer spectroscopy lends further credence to this idea.

A plausible pathway for the formation of the putative resting state species **4-L** would be hydrogenation of  $P_3^BFe-N_2$  by evolved  $H_2$  side-product during catalysis. This process has been demonstrated independently at room temperature in benzene.<sup>29</sup> Follow-up control experiments in  $d_8$ -toluene, however, suggest that this reaction is not kinetically competent at  $-78$  °C. One alternative pathway for the formation of **4-L** during catalysis via bimolecular H-atom transfer from the unobserved intermediate  $P_3^BFe-N_2H$  (e.g.,  $2 P_3^BFe-N_2H \rightarrow$  **4-L** +  $P_3^BFe-N_2$ ), a process that could compete with productive protonation to generate  $P_3^BFe=N-NH_2^+$ . Efforts are ongoing to find conditions under which  $P_3^BFe-N_2H$  can be generated, characterized, and studied.

### 3. CONCLUSION

In the present study we have shown that  $N_2$ -fixing catalyst systems with  $P_3^EFe$  (E = B, C, Si) species give rise to high yields of  $NH_3$  if supplied with sufficient acid and reductant. These yields (for E = B and C) compare very favorably to the most active known Mo catalysts and are almost an order of magnitude greater than the yields presented in our previous reports. While we do not rule out some degree of catalyst degradation at  $-78$  °C, these iron catalysts are unexpectedly robust and it is possible that the lower efficiency of

catalysis at higher turnover is in part due to build-up of  $\text{NH}_3$  product, which is an inhibitor. We have also provided new mechanistic insights for reactions with catalyst  $\text{P}_3^{\text{B}}\text{Fe-N}_2^-$  **1**, such as the observation that catalysis proceeds at  $-78$  °C, the demonstration of first-order rate dependence on catalyst concentration, the demonstration of zeroth-order rate dependence on  $\text{HBAr}^{\text{F}}_4$  concentration, and the observation that **1** catalyzes HER as well as  $\text{NH}_3$  formation. Preliminary electrochemistry data suggests that catalysis by the  $\text{P}_3^{\text{B}}\text{Fe}$  system can be driven at the formal  $\text{P}_3^{\text{B}}\text{Fe-N}_2/\text{P}_3^{\text{B}}\text{Fe-N}_2^-$  couple around  $-2.2$  V vs  $\text{Fc}/\text{Fc}^+$ , consistent with  $\text{Na}/\text{Hg}$  also serving as a viable reductant for catalytic turnover. Cyclic voltammetry and controlled potential electrolysis of  $\text{P}_3^{\text{B}}\text{Fe}^+$  at  $-45$  °C demonstrate that electrolytic  $\text{N}_2$  reduction is possible.

The present study has also demonstrated the utility of coupling in situ freeze-quench  $^{57}\text{Fe}$  Mössbauer spectroscopy with kinetic analysis of product formation as a powerful tool for the mechanistic study of Fe-catalyzed  $\text{N}_2$  fixation. To date, no synthetic molecular  $\text{N}_2$ -to- $\text{NH}_3$  conversion catalyst system had been studied spectroscopically under active turnover conditions. Our freeze-quench Mössbauer results suggest that **4-L** is a resting state of the overall catalysis; this hydride species, which we previously posited to be primarily a catalyst sink, can instead reenter the catalytic pathway via its conversion to catalytically active  $\text{P}_3^{\text{B}}\text{Fe-N}_2^-$  **1**. This observation underscores the importance of understanding metal hydride reactivity in the context of Fe-mediated nitrogen fixation. It may be that HER activity provides a viable strategy for recovering catalytically active states from the unavoidable generation of iron hydride intermediates.

## Supplementary Material

Refer to Web version on PubMed Central for supplementary material.

## Acknowledgments

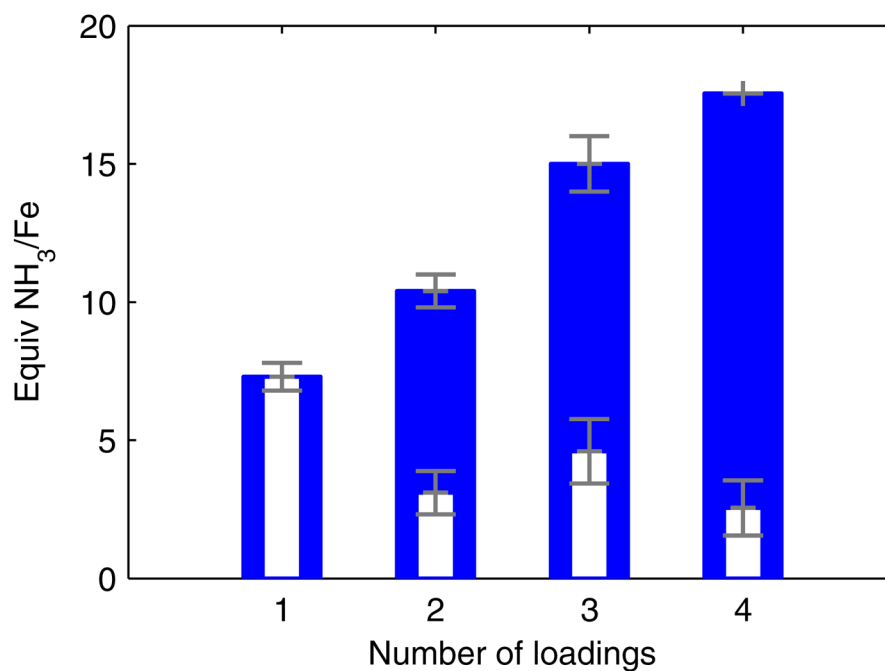
This work was supported by the NIH (GM 070757) and the Gordon and Betty Moore Foundation. T.J.D.C. acknowledges the support of the NSF for a Graduate Fellowship (GRFP) and N.B.T. acknowledges the support of the Resnick Sustainability Institute at Caltech for a Graduate Fellowship.

## References

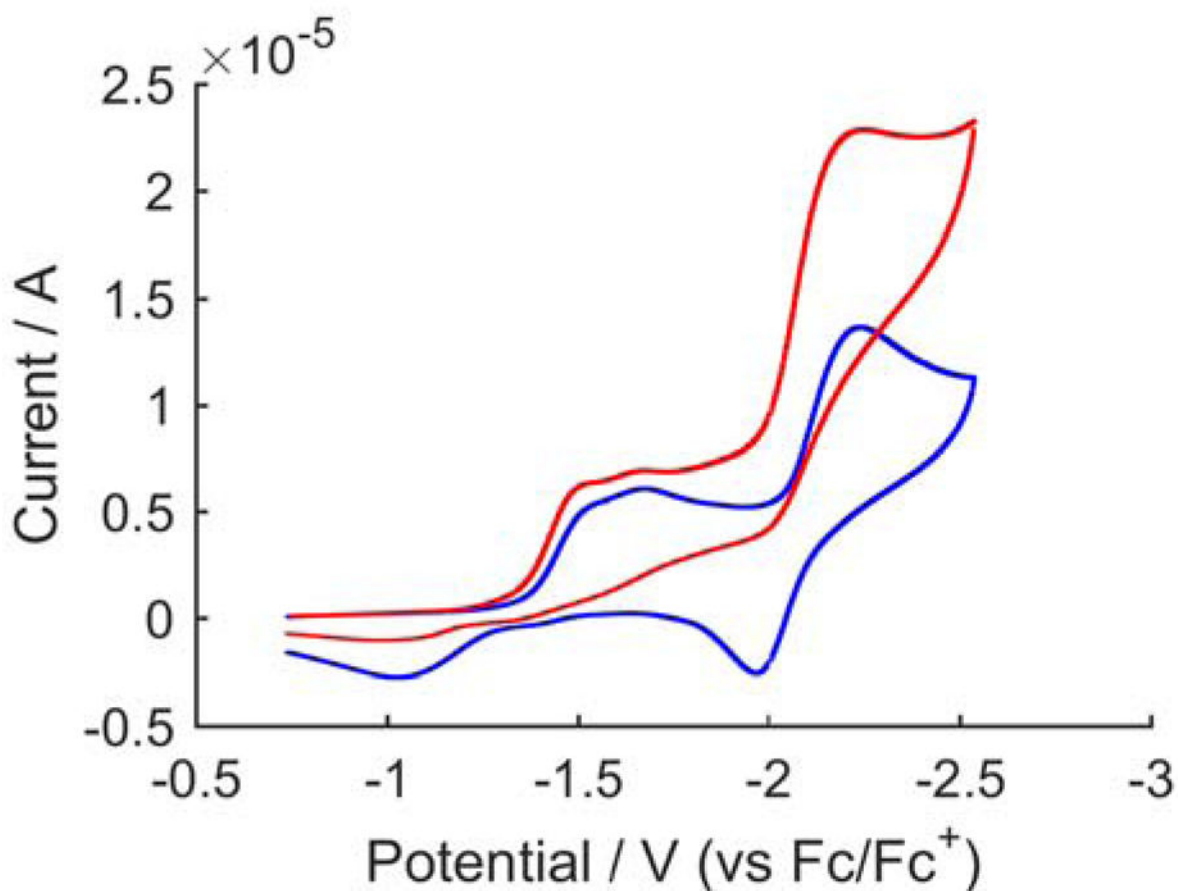
1. Smil, V. *Enriching the Earth*. Cambridge: MIT Press; 2001.
2. (a) Ertl G. *J Vac Sci Technol A*. 1983; 1:1247.(b) Ertl G. *Angew Chem Int Ed*. 2008; 47:3524.
3. Burgess BK, Lowe DJ. *Chem Rev*. 1996; 96:2983. [PubMed: 11848849]
4. (a) Howard JB, Rees DC. *Chem Rev*. 1996; 96:2965. [PubMed: 11848848] (b) Einsle O, Tezcan FA, Andrade SLA, Schmid B, Yoshida M, Howard JB, Rees DC. *Science*. 2002; 297:1696. [PubMed: 12215645] (c) Spatzal T, Aksoyoglu M, Zhang L, Andrade SLA, Schleicher E, Weber S, Rees DC, Einsle O. *Science*. 2011; 334:940. [PubMed: 22096190] (d) Kowalska J, DeBeer S. *Biochim Biophys Acta-Molecular Cell Research*. 2015; 1853:1406.
5. Hoffman BM, Lukoyanov D, Yang ZY, Dean DR, Seefeldt LC. *Chem Rev*. 2014; 114:4041. [PubMed: 24467365]
6. (a) Chatt J, Leigh GJ. *Chem Soc Rev*. 1972; 1:121.(b) Khoenkhoen N, de Bruin B, Reek JNH, Dzik WI. *Eur J Inorg Chem*. 2015; 4:567.
7. Bazhenova TA, Shilov AE. *Coord Chem Rev*. 1995; 144:69.

8. (a) Shiina K. *J Am Chem Soc.* 1972; 94:9266.(b) Komori K, Oshita H, Mizobe Y, Hidai M. *J Am Chem Soc.* 1989; 111:1939.(c) Tanaka H, Sasada A, Kouno T, Yuki M, Miyake Y, Nakanishi H, Nishibayashi Y, Yoshizawa K. *J Am Chem Soc.* 2011; 133:3498. [PubMed: 21341772] (d) Yuki M, Tanaka H, Sasaki K, Miyake Y, Yoshizawa K, Nishibayashi Y. *Nat Commun.* 2012; 3:1254. [PubMed: 23212383] (e) Ogawa T, Kajita Y, Wasada-Tsutsui Y, Wasada H, Masuda H. *Inorg Chem.* 2013; 52:182. [PubMed: 23231761] (f) Liao Q, Saffon-Merceron N, Mézailles N. *Angew Chem Int Ed.* 2014; 53:14206.(g) Ung G, Peters JC. *Angew Chem Int Ed.* 2015; 54:532.(h) Siedschlag RB, Bernales V, Vogiatzis KD, Planas N, Clouston LJ, Bill E, Gagliardi L, Lu CC. *J Am Chem Soc.* 2015; 137:4638. [PubMed: 25799204]
9. (a) Yandulov DV, Schrock RR. *Science.* 2003; 301:76. [PubMed: 12843387] (b) Ritleng V, Yandulov DM, Weare WW, Schrock RR, Hock AS, Davis WM. *J Am Chem Soc.* 2004; 126:6150. [PubMed: 15137780]
10. (a) Arashiba K, Miyake Y, Nishibayashi Y. *Nat Chem.* 2011; 3:120. [PubMed: 21258384] (b) Tanka H, Arashiba K, Kuriyama S, Sasada A, Nakajima K, Yoshizawa K, Nishibayashi K. *Nat Commun.* 2014; 5:3737. [PubMed: 24769530] (c) Kuriyama S, Arashiba K, Nakajima K, Tanaka H, Kamaru N, Yoshizawa K, Nishibayashi Y. *J Am Chem Soc.* 2014; 136:9719. [PubMed: 24896850]
11. Arashiba K, Kinoshita E, Kuriyama S, Eizawa A, Nakajima K, Tanaka H, Yoshizawa K, Nishibayashi Y. *J Am Chem Soc.* 2015; 137:5666. [PubMed: 25879994]
12. (a) Anderson JS, Rittle J, Peters JC. *Nature.* 2013; 501:84. [PubMed: 24005414] (b) Creutz S, Peters JC. *J Am Chem Soc.* 2014; 136:1105. [PubMed: 24350667] (c) Del Castillo TJ, Thompson NB, Suess DLM, Ung G, Peters JC. *Inorg Chem.* 2015; 54:9256. [PubMed: 26001022]
13. Schrock RR. *Angew Chem Int Ed.* 2008; 47:5512.
14. For theoretical work regarding the (PNP)Mo system developed by Nishibayashi, see references 10b,c and also Tian YH, Pierpont AW, Batista ER. *Inorg Chem.* 2014; 53:4177. [PubMed: 24679106]
15. See for example: McWilliams SF, Holland PL. *Acc Chem Res.* 2015; 48:2059–2065. [PubMed: 26099821] Field LD, Li HL, Dalgarno SJ, Turner P. *Chem Commun.* 2008:1680–1682. Crossland JL, Tyler DR. *Coord Chem Rev.* 2010; 254:1883–1894. Peters JC, Mehn MP. *Bio-Organometallic Approaches to Nitrogen Fixation. Activation of Small Molecules.* Tolman WB. Wiley-VCH Weinheim, Germany 2006:81. Hendrich MP, Gunderson W, Behan RK, Green MT, Mehn MP, Betley TA, Lu CC, Peters JC. *Proc Natl Acad Sci U S A.* 2006; 103:17107–17112. [PubMed: 17090681] Grubel K, Brennessel WW, Mercado BQ, Holland PL. *J Am Chem Soc.* 2014; 136:16807. [PubMed: 25412468]
16. (a) Mankad NP, Whited MT, Peters JC. *Angew Chem Int Ed.* 2007; 46:5768.(b) Lee Y, Mankad NP, Peters JC. *Nature Chem.* 2010; 2:558. [PubMed: 20571574]
17. (a) Moret ME, Peters JC. *Angew Chem Int Ed.* 2011; 50:2063.(b) Moret ME, Peters JC. *J Am Chem Soc.* 2011; 133:18118. [PubMed: 22008018] (c) Anderson JS, Moret ME, Peters JC. *J Am Chem Soc.* 2013; 135:534. [PubMed: 23259776]
18. Anderson JS, Cutsail G III, Rittle J, Connor B, Gunderson W, Zhang L, Hoffman B, Peters JC. *J Am Chem Soc.* 2015; 137:7803. [PubMed: 26000443]
19. (a) Krebs C, Price JC, Baldwin J, Saleh L, Green MT, Bollinger JM. *Inorg Chem.* 2005; 44:742. [PubMed: 15859243] (b) Krebs C, Bollinger JM. *Photosynth Res.* 2009; 102:295. [PubMed: 19238577]
20. (a) McLean PA, Papaefthymiou V, Orme-Johnson WH, Münck E. *J Biol Chem.* 1987; 262:12900. [PubMed: 2820958] (b) Yoo SJ, Angove HC, Papaefthymiou V, Burgess BK, Münck E. *J Am Chem Soc.* 2000; 122:4926.
21. Data were not collected at  $-78\text{ }^{\circ}\text{C}$  due to lower solubility of  $\text{NaBAR}^{\text{F}}_4$  at that temperature.
22. Lowe DJ, Thorneley RNF. *Biochem J.* 1984; 224:877. [PubMed: 6395861]
23. This represents a lower limit of the  $\text{H}_2$  produced due to leakage using a set-up that enables quantification of  $\text{H}_2$  and  $\text{NH}_3$  in a single experiment.
24. (a) Daifuku SL, Al-Afyouni MH, Snyder BER, Kneebone JL, Neidig ML. *J Am Chem Soc.* 2014; 136:9132. [PubMed: 24918160] (b) Daifuku SL, Kneebone JL, Snyder BER, Neidig ML. *J Am Chem Soc.* 2015; 137:11432. [PubMed: 26266698]

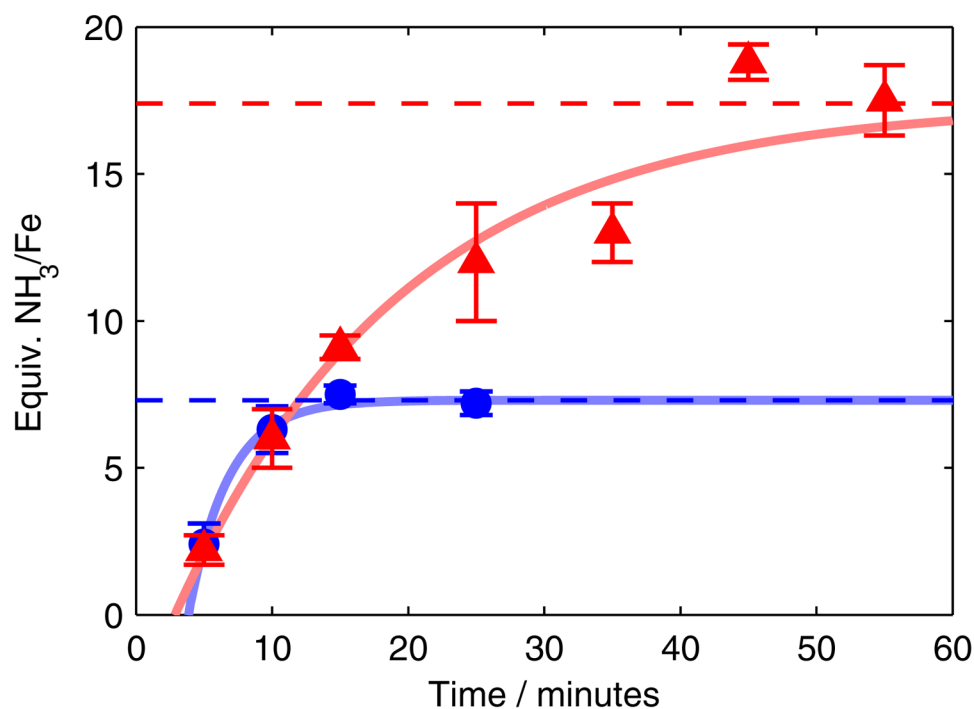
25. Berry JF, Bill E, Bothe E, DeBeer S, Mienert B, Neese F, Wieghardt K. *Science*. 2006; 312:1937. [PubMed: 16741074]
26. Lee Y, Peters JC. *J Am Chem Soc*. 2011; 133:4438. [PubMed: 21375250]
27. Ye S, Bill E, Neese F. *Inorg Chem*. 2016; ASAP. doi: 10.1021/acs.inorgchem.5b02908
28. If the adamantyl imide species  $P_3^BFe-NAd^{0/1+}$  are excluded from the series of data collected in Figure 6, the correlation improves significantly ( $r^2 = 0.96$ ). The isomer shifts of these imides appear to be systematically reduced by ca. 0.1–0.2 mm s<sup>-1</sup> from the trend exhibited by the rest of the compounds in Table 3.
29. Fong H, Moret ME, Lee Y, Peters JC. *Organometallics*. 2013; 32:3053. [PubMed: 24000270]
30. Münck E. *Methods Enzymol*. 1978; 54:346. [PubMed: 215877]
31. Although the low isomer shift of the minor component present in Figure 7B is suggestive of a diamagnetic ground state, its identity is presently unknown.
32. Also present in Figure 8A: ca. 20% of the species with parameters  $\delta = -0.03 \pm 0.04$  mm s<sup>-1</sup> and  $E_Q = 2.88 \pm 0.09$  mm s<sup>-1</sup> that is present in Figure 7C (white), and ca. 20% of a broad residual signal consistent with an unresolved quartet species (grey). Also present in Figure 8B: ca. 20% of neutral  $P_3^BFe-N_2$  (green); ca. 15% of a sharply resolved species with parameters  $\delta = 0.68$  mm s<sup>-1</sup> and  $E_Q = 1.40$  mm s<sup>-1</sup> (white) that is consistent with a quartet species such as  $P_3^BFe-NH_2$ ; ca. 20% of a broad residual signal consistent with an unresolved quartet species (grey).
33. Also present in Figure 8C: ca. 10% of the species with parameters  $\delta = -0.03 \pm 0.04$  mm s<sup>-1</sup> and  $E_Q = 2.88 \pm 0.09$  mm s<sup>-1</sup> that is present in Figure 7C and 8A (white), and ca. 15% of a broad residual signal consistent with an unresolved quartet species (grey).
34. (a) Lowe DJ, Thorneley RNF. *Biochem J*. 1984; 224:887. [PubMed: 6395862] (a) Lowe DJ, Thorneley RNF. *Biochem J*. 1984; 224:895. [PubMed: 6395863] (a) Lowe DJ, Thorneley RNF. *Biochem J*. 1984; 224:903. [PubMed: 6395864]
35. Lukoyanov D, Yang ZY, Khadka N, Dean DR, Seefeldt LC, Hoffman BM. *J Am Chem Soc*. 2015; 137:3610. [PubMed: 25741750]
36. (a) Rivera-Ortiz JM, Burris RH. *J Bacteriol*. 1975; 123:537. [PubMed: 1150625] (b) Simpson FB, Burris RH. *Science*. 1984; 224:1095. [PubMed: 6585956]
37. Rittle J, Peters JC. *J Am Chem Soc*. 2016; online ASAP. doi: 10.1021/jacs.6b01230



**Figure 1.** Yields of NH<sub>3</sub> obtained using P<sub>3</sub><sup>B</sup>Fe-N<sub>2</sub><sup>-</sup> **1** from successive reloading of HBAr<sup>F</sup><sub>4</sub> and KC<sub>8</sub> to reactions maintained at -70 °C in Et<sub>2</sub>O. Blue bars denote total observed yields and white inset bars denote the average increase in total yield from the final loading of substrate. Each loading corresponds to 48 equiv HBAr<sup>F</sup><sub>4</sub> and 58 equiv KC<sub>8</sub> relative to Fe. Data presented are averages of two experiments.

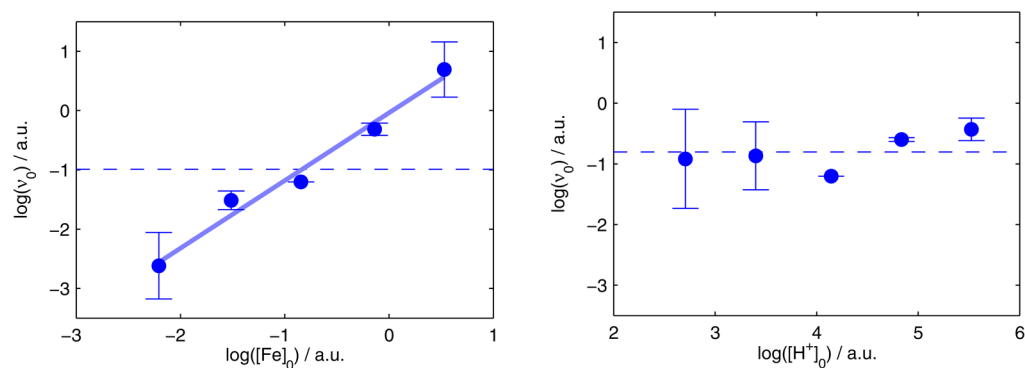


**Figure 2.** Cyclic voltammetry of  $[\text{P}_3^{\text{B}}\text{Fe}][\text{BARF}_4]$  in the presence of 0 (blue trace) and 5 (red trace) equiv  $\text{HBARF}_4$ , collected in  $\text{Et}_2\text{O}$  with 0.1 M  $\text{NaBARF}_4$  electrolyte at  $-45^\circ\text{C}$  using a glassy carbon electrode and referenced to the  $\text{Fc}/\text{Fc}^+$  couple. Scan rate is 100 mV/s.



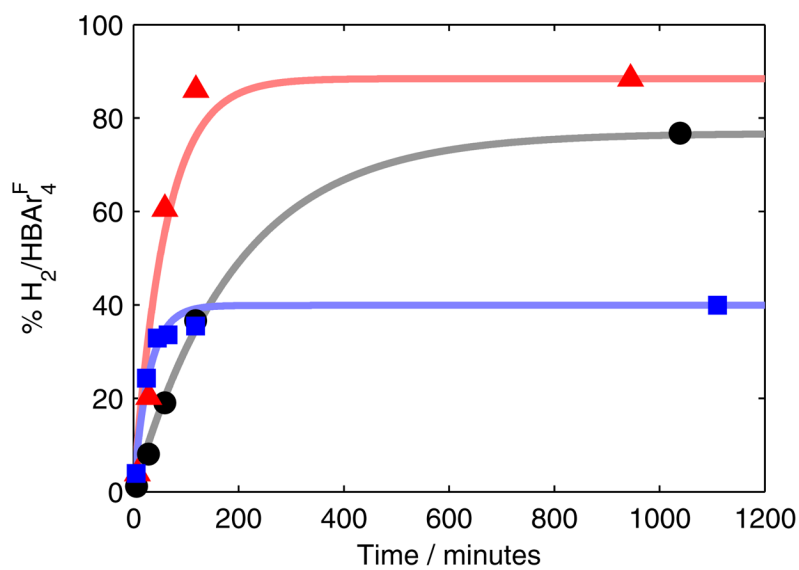
**Figure 3.**

Time profiles of the formation of  $\text{NH}_3$  from  $\text{N}_2$  using **1** as a catalyst at  $-78\text{ }^\circ\text{C}$  under previously reported reaction conditions (blue circles,  $0.64\text{ mM}$  **1**, 48 equiv  $\text{HBAr}^{\text{F}_4}$ , 58 equiv  $\text{KC}_8$ ) and higher-turnover conditions (red triangles,  $0.43\text{ mM}$  **1**, 150 equiv  $\text{HBAr}^{\text{F}_4}$ , 185 equiv  $\text{KC}_8$ ). Dashed lines show expected final yields from the corresponding entries in Table 1 (Entries 1 and 3). Each point represents an average of two experiments; data for the individual experimental iterations are presented in the Supporting Information. Solid lines are provided as guides for the eye only.

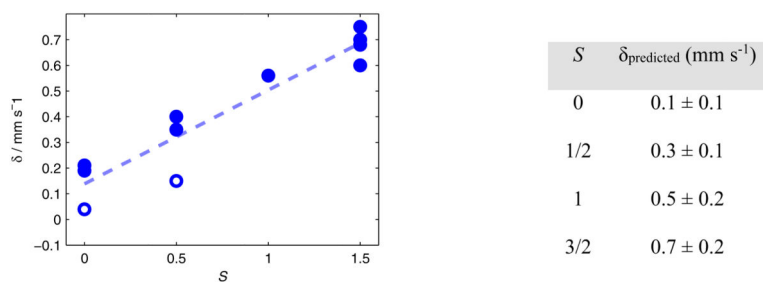


**Figure 4.**

Log-log plots of the initial rate of  $\text{NH}_3$  formation ( $v_0$ ) versus initial concentrations of soluble reagents. (Left)  $v_0$  versus  $[\text{Fe}]_0$  for a range of  $[\mathbf{1}]$  from 0.11–1.7 mM. The dashed line shows a constant function fit to the mean of the data, while the solid trend line shows the result of least squares linear regression ( $\log(v_0) = (-0.04 \pm 0.1) + (1.1 \pm 0.1) \cdot \log([\mathbf{1}]_0)$ ,  $r^2 = 0.98$ ). (Right)  $v_0$  versus  $[\text{HBAr}^{\text{F}}_4]_0$  for a range of  $[\text{HBAr}^{\text{F}}_4]$  from 15–250 mM. The dashed line shows a constant function fit to the mean of the data (RMSE = 0.3), which is not statistically different from the result of a least squares linear regression (RMSE = 0.3). Data for individual experimental iterations and discussion of initial rates estimates are presented in the Supporting Information.

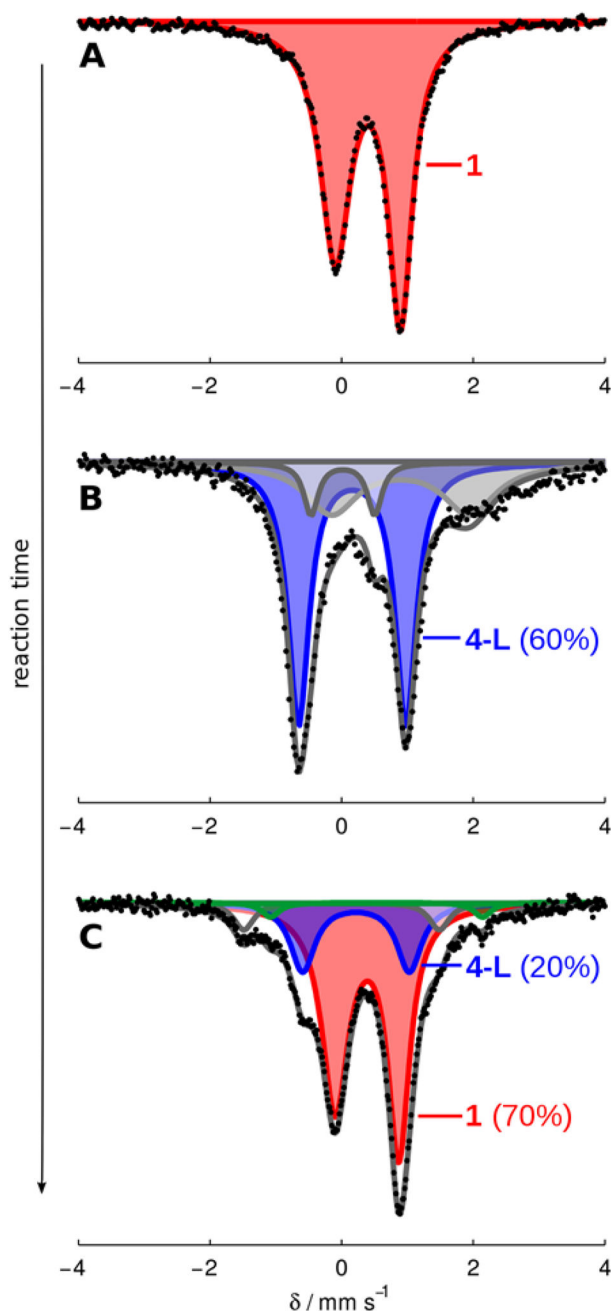


**Figure 5.** Time profiles of the formation of H<sub>2</sub> from HBAr<sup>F</sup><sub>4</sub> and KC<sub>8</sub> in Et<sub>2</sub>O at -78 °C. Data is presented for the reaction of these reagents alone (black circles) as well as in the presence of **1** (blue squares) and **3** (red triangles). Each time course was collected continuously from a single experiment. Solid lines are provided as guides for the eye only.

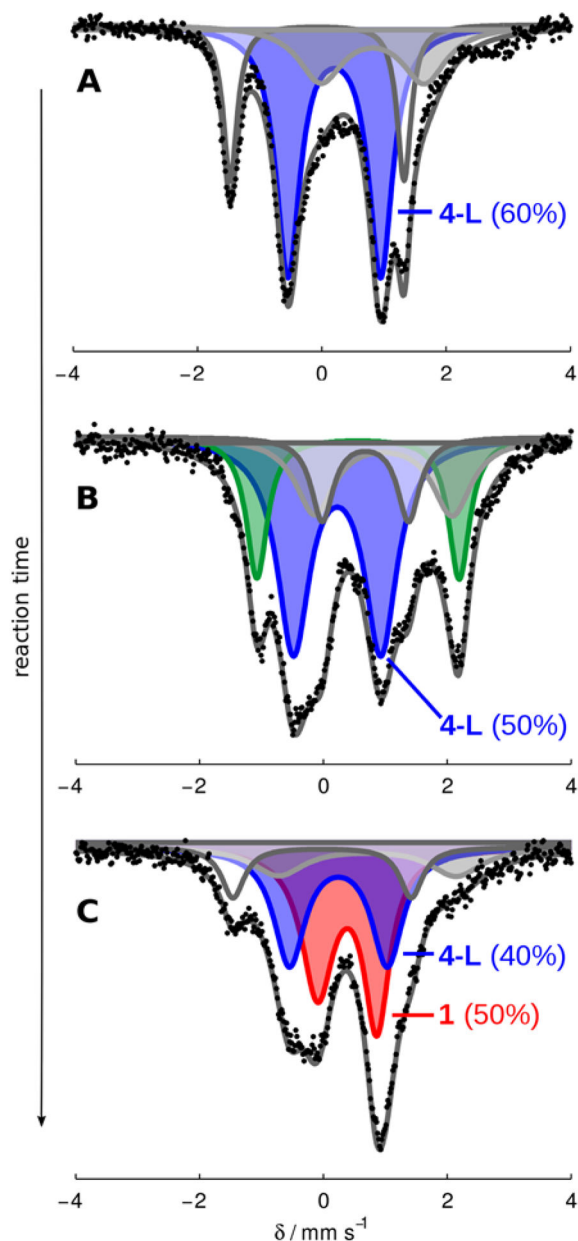


**Figure 6.**

A plot of  $\delta$  versus ground spin-state  $S$  for the compounds listed in Table 3 (blue circles), along with a linear least-squares fit to the data (dotted line,  $r^2 = 0.90$ ). The isomer shifts of the  $\text{P}_3\text{BFe-NAAd}^{0/1+}$  are highlighted by open circles.<sup>28</sup> The table to the right lists the expectation values for  $\delta$  based on  $S$  computed from the linear fit (ranges reported as 95% confidence interval).

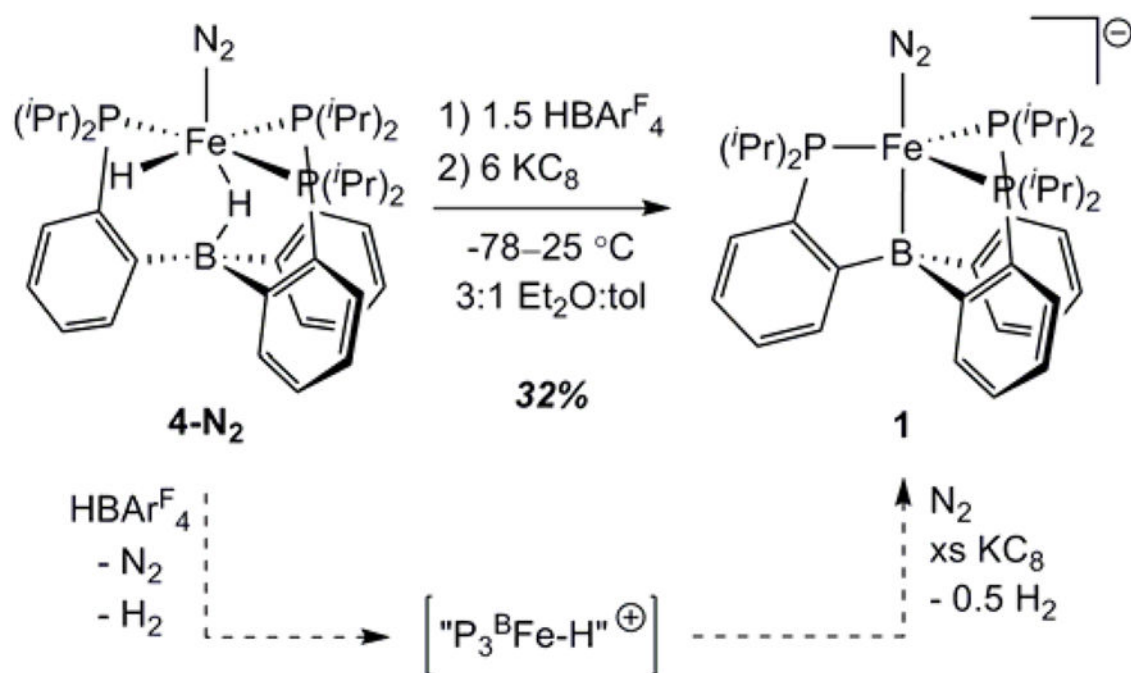


**Figure 7.** Frozen solution Mössbauer spectra collected at 80 K in the presence of a 50 mT parallel magnetic field. (A) Spectrum of **1** (0.64 mM in THF); (B) a catalytic mixture (Et<sub>2</sub>O, 0.64 mM **1**, 48 equiv HBAr<sup>F</sup><sub>4</sub>, 58 equiv KC<sub>8</sub>) freeze-quenched after 5 minutes of stirring at -78 °C; (C) a catalytic mixture (Et<sub>2</sub>O, 0.64 mM **1**, 48 equiv HBAr<sup>F</sup><sub>4</sub>, 58 equiv KC<sub>8</sub>) freeze-quenched after 25 minutes of stirring at -78 °C. Data are presented as black points and simulations as solid grey lines with components plotted as solid areas underneath the curve. For parameters of individual components see the SI.



**Figure 8.**

Frozen solution Mössbauer spectra collected at 80 K in the presence of a 50 mT parallel magnetic field. (A) A catalytic mixture ( $\text{Et}_2\text{O}$ , 0.43 mM **1**, 150 equiv  $\text{HBAr}^{\text{F}_4}$ , 185 equiv  $\text{KC}_8$ ) freeze-quenched after 5 minutes of stirring at  $-78\text{ }^\circ\text{C}$ ; (B) a catalytic mixture ( $\text{Et}_2\text{O}$ , 0.43 mM **1**, 150 equiv  $\text{HBAr}^{\text{F}_4}$ , 185 equiv  $\text{KC}_8$ ) freeze-quenched after 10 minutes of stirring at  $-78\text{ }^\circ\text{C}$ ; (C) a catalytic mixture ( $\text{Et}_2\text{O}$ , 0.43 mM **1**, 150 equiv  $\text{HBAr}^{\text{F}_4}$ , 185 equiv  $\text{KC}_8$ ) freeze-quenched after 25 minutes of stirring at  $-78\text{ }^\circ\text{C}$ . Data presented as black points, simulations as solid grey lines with components plotted as solid areas underneath the curve. For parameters of individual components, see SI.

**Scheme 1.**

Stoichiometric conversion of **4-N<sub>2</sub>** into **1** under catalytically relevant conditions. A proposed reaction pathway is shown along the dashed arrows. “P<sub>3</sub>BFe-H<sup>+</sup>” is a plausible intermediate of this conversion but has not been thoroughly characterized.



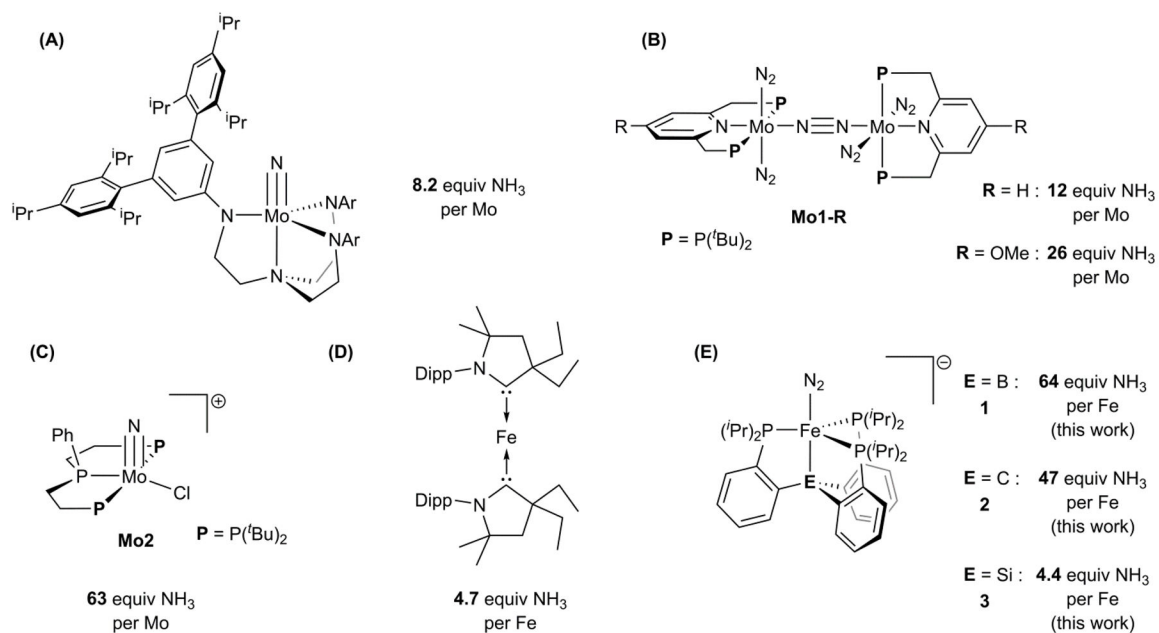


**Chart 1. Synthetic catalysts for nitrogen fixation with maximum observed yields of  $\text{NH}_3$ <sup>a</sup>**

<sup>a</sup>(A) See reference 9a. (B) See references 10. (C) See reference 11. (D) See reference 8g. (E) See references 12. Note that  $\text{NH}_3$  equivalents shown represent the highest single-run values that have been reported for the various catalysts shown; direct cross-comparisons of Fe and Mo catalyst performance are tenuous due to the different reaction conditions used.

Table 1

NH<sub>3</sub> Generation from N<sub>2</sub> Mediated by Synthetic Fe Catalysts<sup>a</sup>

$$\text{N}_2 + [\text{H}(\text{OEt}_2)_2][\text{BAr}^{\text{F}}_4] + \text{KC}_8 \xrightarrow[\text{Et}_2\text{O}]{\text{catalyst}} \text{NH}_3$$

-78 °C

Entry	Catalyst	[Fe] (mM)	HBAr <sup>F</sup> <sub>4</sub> equiv	KC <sub>8</sub> equiv	Variation	Equiv NH <sub>3</sub> /Fe	% Yield NH <sub>3</sub> /H <sup>+</sup>
1	<b>1</b>	1.3	48	58	—	7.3 ± 0.5	45 ± 3
2	<b>1</b>	0.64	96	58	—	12 ± 1	38 ± 3
3	<b>1</b>	0.43	150	185	—	17.4 ± 0.2	35.6 ± 0.4
4	<b>1</b>	0.08	720	860	—	43 ± 4	18 ± 2
5	<b>1</b>	0.04	1500	1800	—	59 ± 6	12 ± 1
6 <sup>b</sup>	<b>2</b>	1.0	37	40	[HBAr <sup>F</sup> <sub>4</sub> ] = 31 mM	4.6 ± 0.8	36 ± 6
7	<b>2</b>	0.56	110	120	—	11.3 ± 0.9	31 ± 2
8	<b>2</b>	0.28	220	230	—	14 ± 3	19 ± 4
9	<b>2</b>	0.08	750	810	—	19 ± 4	7 ± 2
10	<b>2</b>	0.04	1500	1600	—	36 ± 7	7 ± 1
11 <sup>c</sup>	<b>3</b>	0.58	48	58	[HBAr <sup>F</sup> <sub>4</sub> ] = 31 mM	0.8 ± 0.5	5 ± 3
12	<b>3</b>	0.04	1500	1800	—	3.8 ± 0.8	0.8 ± 0.2
13	<b>4-N<sub>2</sub></b> <sup>d</sup>	-	150	185	3% toluene	1.1 ± 0.1	2.4 ± 0.3
14	<b>4-N<sub>2</sub></b>	0.44	150	185	25% toluene	5.6 ± 0.9	12 ± 2
15	<b>1</b>	0.41	150	185	25 equiv NH <sub>3</sub> added	6.4 ± 0.1	13.2 ± 0.2
16	<b>1</b>	0.41	150	0	1900 equiv 10 wt% Na/Hg	5.0 ± 0.2	10.3 ± 0.5

<sup>a</sup>Fe precursor, HBAr<sup>F</sup><sub>4</sub>, KC<sub>8</sub>, and Et<sub>2</sub>O sealed in a vessel at -196 °C under an N<sub>2</sub> atmosphere followed by warming to -78 °C and stirring at -78 °C. Unless noted otherwise, [HBAr<sup>F</sup><sub>4</sub>] = 63 mM. Yields are reported as an average of at least 2 iterations; data for individual experimental iterations are presented in the Supporting Information.

<sup>b</sup>Data taken from reference 12b.

<sup>c</sup>Data taken from reference 12a.

<sup>d</sup>Not fully soluble under reaction conditions.

**Table 2**Comparison of NH<sub>3</sub> Generating Reactions<sup>a</sup>

Catalyst	Temperature (°C)	Maximum yield <sup>d</sup>	TOF (min <sup>-1</sup> )	Efficiency (%)
<b>Mo1-H</b> <sup>a</sup>	25	12	0.14	31
<b>Mo2</b> <sup>b</sup>	25	63	0.26	35
<b>1</b> <sup>c</sup>	-78	64	1.2	12

Data for **Mo1-H** and **Mo2** are from reference 11 and depictions of the compounds are presented in Chart 1.

<sup>a</sup>Conditions: 2,6-lutidinium trifluoromethanesulfonate and cobaltocene in toluene.

<sup>b</sup>Conditions: 2,4,6-trimethylpyridinium trifluoromethanesulfonate and decamethylcobaltocene in toluene.

<sup>c</sup>Conditions: HBAr<sub>4</sub><sup>F</sup> and KC8 in diethyl ether.

<sup>d</sup>Expressed in NH<sub>3</sub> equivalents.

**Table 3**Mössbauer parameters for  $P_3^BFe$  complexes<sup>a</sup>

Compound	S	Conditions	$\delta$ (mm s <sup>-1</sup> )	$E_Q$ (mm s <sup>-1</sup> )
$P_3^BFe^{+b}$	3/2	Frozen solution, 50 mT	0.75	2.55
$P_3^BFe-N_2H_4^+$	3/2	Frozen solution, 50 mT	0.7	2.30
$P_3^BFe-NH_3^+$	3/2	Frozen solution, zero field	0.68	1.94
$P_3^BFe-NH_2$	3/2	Frozen solution, zero field	0.60	1.47
$P_3^BFe-N_2^b$	1	Frozen solution, 50 mT	0.56	3.34
$P_3^BFe-N_2^-b$	1/2	Frozen solution, 50 mT	0.40	0.99
$P_3^BFe-NNH_2^+b$	1/2	Frozen solution, 50 mT	0.35	1.02
$P_3^BFe-NAd^+$	1/2	Powder, 50 mT	0.15	1.31
$(P_3^B)(\mu-H)Fe(H)(N_2)$	0	Frozen solution, zero field	0.21	1.44
$(P_3^B)(\mu-H)Fe(H)(H_2)$	0	Frozen solution, zero field	0.19	1.55
$P_3^BFe-NAd$	0	Powder, zero field	0.04	1.40

<sup>a</sup>All data were collected at 80 K under the conditions noted; external magnetic fields applied in parallel mode.<sup>b</sup>Data taken from reference 18.